Transport of topological edge states in 2D Zigzag edge Tungsten Ditelluride Nanoribbon

Joy Sharma . Nishat Mahzabin Helaly . Mahabub Alam

Bangladesh University of Engineering and Technology , Bangladesh

Abstract

In this paper, we have investigated the transport of topological edge states in 2D Zigzag edge Tungsten Ditelluride Nanoribbon (ZTDNR). We have found that zigzag edge nanoribbon (NR) of Tungsten Ditelluride develops topological edge states in the presence of intrinsic spin orbit interaction (SOC). We have used three band tight binding model for the electrons of d_{z^2}, d_{xy}, and $d_{x^2-y^2}$ orbitals with SOC for calculating band structure of NR and Non Equilibrium Greens Function (NEGF) formalism for transport in the NR. We have investigated transport in a pristine device, transport in the presence of a finite potential barrier, transport with constriction within the device and transport with edge imperfections.

Keywords:

Topological Insulator, Spin orbit coupling, Tungsten ditelluride, Non-equilibrium greens function, Nanoribbon.

1. Introduction

Two-dimensional materials([1]-[4]) are attractive for their use in next-generation nanoelectronic and optoelectronic devices because, compared to one-dimensional materials, it is relatively easy to fabricate complex structures from them. Recently a new class of two-dimensional (2D) materials—the monolayer transition metal dichalcogenides (TMD) ([5]-[7]) has received great attention for their significant potential as the channel material in emerging nanoelectronic devices. 2D TMDs exhibit many rich properties such as excellent mobility [8] at room temperature, the unsaturated magneto resistance, gas sensor ([9]-[10]), FET([11]-[12]), memoristor [13] and super conductivity [14] making them promising candidates for electronic and optoelectronic applications.

Some TMDs have been theoretically and experimentally proven as topological insulator. In 2D topological insulators (TI), the nontrivial edge states support quantum spin Hall (QSH) [15] effect. TI has a pair of edge states of opposite spins where the electrons with opposite spins will propagate along opposite direction. This property enables the topological edge states immune to scattering from non-magnetic impurities([16]-[19]). Since the early proposal of QSH effect in graphene, spin-orbit coupling (SOC) has played a key role to ma-

nipulate the properties of a material. Materials with strong SOC drastically differ from other materials and exhibit some novel phenomena([20]-[21]). So, a number of 2D systems are being examined. A few of them are confirmed experimentally to have large SOC and direct band gap. Among them Tungsten Ditelluride (WTe_2) exhibits properties like having direct bandgap in bulk monolayer, breaking of inversion symmetry due to the trigonal prismatic geometry and the largest SOC strength among TMDs([22]-[23]). These properties render it as a rich and interesting platform to study QSH effect([24]-[25]).

In this study, we have presented the transport properties of 2D Zigzag nanoribbon of WTe_2 confirming it as a topological insulator. We have used three band tight binding model for simulating the monolayer WTe_2 nanoribbon as has been used by other researchers([26]). The parameters of this TB model are obtained by fitting the DFT analysis and used for low energy description of single layered 2D materials([26]). So, This TB model is sufficient to capture the band-edge properties including the energy dispersion. For describing the transport, in this work the NEGF [27] formalism has been used. The transport properties of WTe_2 nanoribbon are studied for different scenarios.

2. Theory

TMDs are referred to generically as MX_2, where M represents the transition metal and X the chalcogen. A monolayer can be seen as a lattice of M and X atoms. Each M (Tungsten,W) atom is connected with neighboring X (Ditelluride,Te) atoms. These materials have two different kinds of unit cells depending on the geometry of the coordination of M atom with the X atoms. One of them has a trigonal prismatic structure where every M atom is connected with six X atoms and it is called $2H$ (hexagonal symmetry) or $3R$ (rhombohedral symmetry). The other one is octahedral coordination. Its structure will be $1T$ (tetragonal symmetry)[28]. In this study, we have considered trigonal prismatic structure($2H$ or hexagonal symmetry), with sites M and X. Figure 1 shows a top-down view of the monolayer crystal structure.

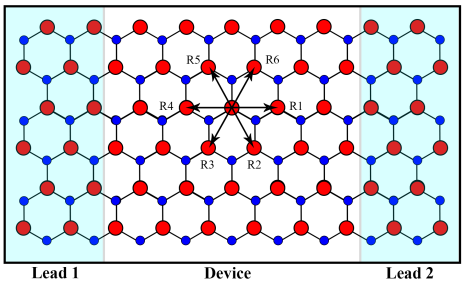

Figure 1: Lattice structure of TMD

For modeling the Hamiltonian of nanoribbon of TMDs , We have considered a three-band tight-binding (TB) model including spin. The conduction and valence-band edges are predominantly contributed by the d_{z^2}, d_{xy} and $d_{x^2-y^2}$ orbitals of M atoms. So the TB model is constructed using these three orbitals based on the symmetries of the monolayers. Due to the heavy transition-metal M atom, TMDs spin orbital coupling can be large. The large SOC of monolayer MX_2 is a fascinating feature. For our study, SOC effects are studied under the approximation of on-site spin-orbit inter-

actions of M atoms. In this paper, we have demonstrated different features of edge states for WTe_2 nano ribbon by altering the device geometry. We have considered constriction, edge imperfection and barrier. In simulation, constriction has been implemented by removing a chunk of atoms at one edge of the NR. Edge imperfections can happen during fabrication process in the NR. We introduced it by removing random atoms from the edge. For demonstrating barrier, we increased the energy of some particular atoms. These transport characteristics of the nanoribbon have been simulated using NEGF formalism. The NEGF formalism enabled us to describe the quantum transport of electron for nanoscale devices.

3. Mathematical model

We have used NEGF formalism in this work. We can calculate electron density and transmittance of the electrons inside a device by using this formalism([29]-[32]). The Green's function, G^R is the impulse response of a device. We can calculate the green's function of the device from the device Hamiltonian, H and the self energies of the interaction i.e. Σ_{l1} (left lead) and Σ_{l2} (right lead). Now the green's function, G^R can be calculated using the following equation([29]-[32]):

$$[EI - H - \Sigma_{l1} - \Sigma_{l2}]G^R = I \tag{1}$$

In the above eq.(1), E is the energy of electrons that are introduced into the device through the lead and I denotes identity matrix. The energy E is around the Fermi energy level of the device. To get Hamiltonian of the device, we have used tight binding model. We can express Hamiltonian through the following equation([33]) :

$$H_o = \sum_i \sum_j a^{\dagger}_{i\alpha} E_{\alpha\beta}(r_{ij}) a_{j\beta}; r_{ij} = r_i - r_j \tag{2}$$

In eq.2, α and β are indices for orbitals. $E_{\alpha\beta}(r_{ij})$ is the next nearest neighbor M-M 3×3 Hamiltonian matrix. We assume r_{ij}=R_l and l=1,2,...6. R_l indicates the next nearest lattice vectors as has been shown in fig.1. The building blocks of H_0 are 3×3 matrices [33]. When we introduce spin-orbit coupling , the building blocks of H become 6×6 matrices. For spin, we use six bases and they are $|d_{z^2},\uparrow>$,$|d_{xy},\uparrow>$,$|d_{x^2-y_2},\uparrow>$,$|d_{z^2},\downarrow>$,$|d_{xy},\downarrow>$,$|d_{x^2-y_2},\downarrow>$. There are three up spin bands and three down spin bands [30]. Now we can get the SOC contribution to the Hamiltonian as([33]):

$$H^{'} = \lambda L.S = \frac{\lambda}{2}\begin{bmatrix} L_z & 0 \\ 0 & -L_z \end{bmatrix} \tag{3}$$

where,

$$L_z = \begin{bmatrix} 0 & 0 & 0 \\ 0 & 0 & 2i \\ 0 & -2i & 0 \end{bmatrix} \tag{4}$$

L_z is a matrix of z component of the orbital angular momentum in bases of d_{z^2},d_{xy}, and $d_{x^2-y^2}$and λ characterizes the strength of the SOC. Now we can get the full

TB Hamiltonian with SOC as follows([33]):

$$H = I_2 \otimes H_o + H^{'} = \begin{bmatrix} H_o + \frac{\lambda}{2}L_z & 0 \\ 0 & H_o - \frac{\lambda}{2}L_z \end{bmatrix} \quad (5)$$

In Eq.5, I_2 is the 2×2 indentity matrix and H_o is Hamiltonian of the device without SOC as has been shown in eq.(2).

The electron correlation function, G^n and the hole correlation function, G^P are computed by the following equations ([29]-[32],[34]):

$$G^n = G^R\Sigma^{in}G^A \quad (6)$$

$$G^p = G^R\Sigma^{out}G^A \quad (7)$$

Here $G^A = [G^R]^\dagger$. G^A represents the advanced green function. Σ_{in} and Σ_{out} are the scattering functions. They describe the rate at which electrons are scattered in and out of the device. They can be calculated by the following equations([29]-[31]):

$$\Sigma^{in} = \Sigma^{in}_{l1} + \Sigma^{in}_{l2} \quad (8)$$

$$\Sigma^{out} = \Sigma^{out}_{l1} + \Sigma^{out}_{l2} \quad (9)$$

$$\Sigma^{in}_{l1} = f_1\Gamma_{l1} \quad (10)$$

$$\Sigma^{out}_{l1} = (1 - f_1)\Gamma_{l1} \quad (11)$$

$$\Sigma^{in}_{l2} = f_2\Gamma_{l2} \quad (12)$$

$$\Sigma^{out}_{l2} = (1 - f_2)\Gamma_{l2} \quad (13)$$

$$\Gamma_{l1} = i[\Sigma_{l1} - \Sigma^\dagger_{l1}] \quad (14)$$

$$\Gamma_{l2} = i[\Sigma_{l2} - \Sigma^\dagger_{l2}] \quad (15)$$

In the above equations, f_1 and f_2 denote probability of finding electrons in the left and right lead respectively. The transmittance can also be calculated from the following equation ([32]) :

$$T = trace(\Gamma_{l1}G^R\Gamma_{l2}G^A) \quad (16)$$

4. Result and discussion

4.1. Electronic Band Structure

The electronic band structure of a material allows us to envision the allowed states of electrons in the material. We have presented the electric band structure using three band tight binding model. This model only considers the next nearest neighbour hopping of M(W) atoms. We have shown electronic band structure of ZTDNR in Fig.2. This is for 16-zigzag-ribbon i.e. there are 16 number of atoms in one column (unit cell of NR).

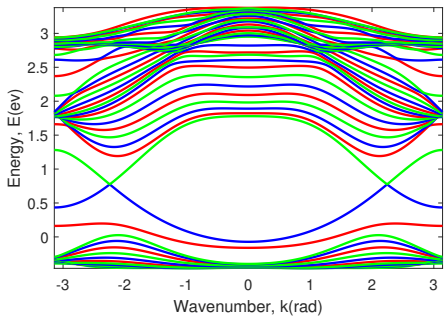

Figure 2: Band Structure of ZTDNR without SOC for one spin

There is an establishment of Dirac cone in fig.2. The blue and green bands in the middle of fig.2 are for d_{z^2} and $d_{x^2-y^2}$ electrons. They describe the energy dispersion relationship of edge states at the two edges of the NR. In fig.3, we have demonstrated the electronic band structure of the NR with SOC effect. From fig.3, we observe that SOC splits the dirac cone and creates a direct band gap among the d_{z^2} and $d_{x^2-y^2}$ bands. There is

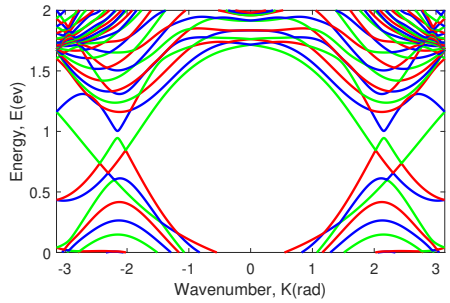

Figure 3: Band Structure of ZTDNR with SOC for both spins

a linear energy region of the $d_{x^2-y^2}$ band represented by the green curve between the direct bandgap. The $d_{x^2-y^2}$ band represents the topological edge state in ZTDNR.

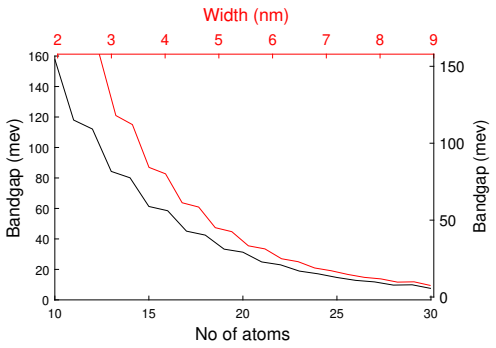

Figure 4: Bandgap (TI region) as a function of width (red curve) and no of atoms (black curve) for ZTDNR with SOC

One of the exciting properties of ZTDNR is to control its direct bandgap. We observe a dependency of the direct bandgap of zigzag NR with the width. From fig.4, it can be said that the bandgap shrinks with the increase of the width of zigzag NR. Modern technologies of fabrication have reached a level where 2D material NR with a particular atomic width can be grown ([35]). Here, we consider sixteen atoms along the width of the NR. It is about 4.624nm wide and has a band gap of approximately 50mev.

Such opening of gap in the metallic part of band structure and concomitant appearance of topological Dirac cone like bands has not been seen in any other material in our knowledge. It can be mentioned that by applying suitable gate voltage it is easier for 2D materials to shift the band structure without changing the Fermi level ([36]). So it is possible to use these topological states for transport of electrons.

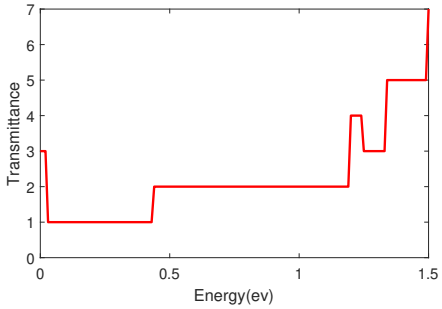

Figure 5: Transmittance vs Energy of ZTDNR without SOC

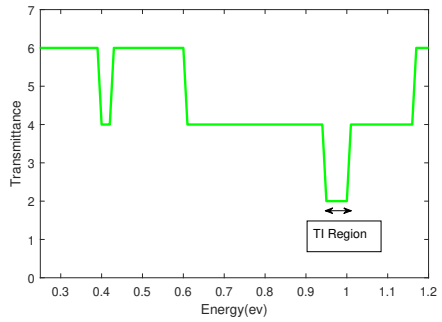

Figure 6: Transmittance vs Energy of ZTDNR with SOC

We have shown two plots of transmittance vs energy without and with SOC in fig.5 and fig.6 respectively. These plots are for 16-ZTDNR. We can observe the increase of transmittance after introducing SOC as shown in fig.6 because we consider up spin and down spin electrons for SOC. But transmittance at an energy range from 0.95ev to 1ev is 2 for two plots. We find topological edge properties at this energy range after introducing

SOC in 16-ZTDNR. So, we are interested to investigate the transport properties at this energy range.

4.2. Transport in a pristine device

In this section, we have investigated the transport property of a pristine device for ZTDNR with SOC. We have found six electron density profiles for ZTDNR. They are three electron density profiles of up spin electrons and three electron density profiles of down spin electrons. In fig.7, we have presented the electron density profile of one of three up spin electrons. In fig.8 we have also shown the electron density profile of one of three down spin electrons.

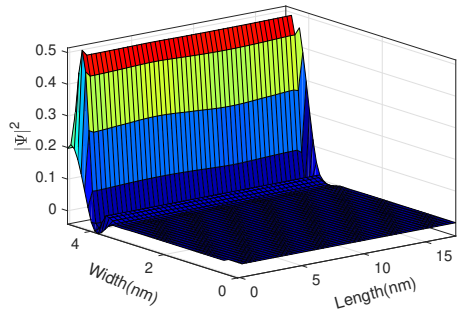

Figure 7: Electron density profile for ZTDNR up spin

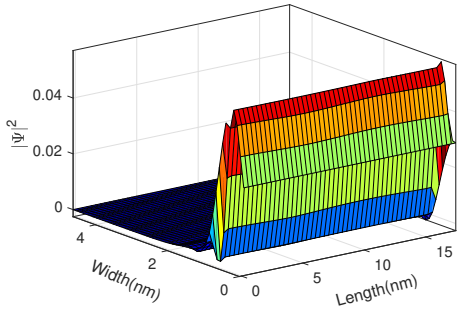

Figure 8: Electron density profile for ZTDNR down spin

Three electron density profiles for each spin electron have electron distribution at same edge of the device. So, we have demonstrated only one electron density profile for each spin electrons. From the figures, we observe finite electron distribution only along one of the edges of the device for a particular spin. For the electron density profiles in fig.7 and fig.8, electrons enter the device through the left lead and leave through the right lead. We have chosen the energy to be 0.98eV. If we change the direction of electrons passing through the device in such a way that electrons are entering the device from the right lead and leaving from left lead, electron density profile will also change from one edge to another. No back scattering occurs for these edge states and these edge states are behaving as quantum spin hall states.

4.3. Transport in the presence of barrier inside the device

In this section, we have investigated the phenomenon of Klein tunneling in the presence of barrier inside the device. Klein tunneling represents a phenomenon in which the electrons can pass through a high potential barrier and transmittance of the electrons is not dependent on the height and width of barrier. Hence transmittance always remains same. Here, we have considered an electron energy 0.975ev which is in the TI energy range for 16-ZTDNR and have put barrier inside the device. We have demonstrated two electron density profiles for up spin electron and down spin electron in fig.9 and in fig.10 respectively.

From the above figures, we observe that electrons can pass through the device and travel with full transmittance (T=2). We have also increased the height and

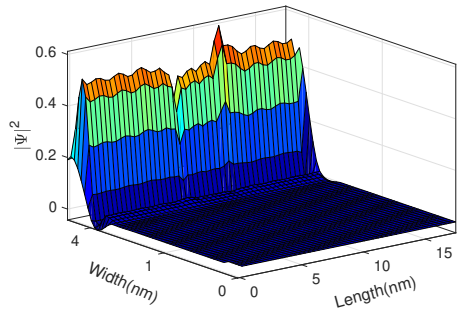

Figure 9: Electron density profile for ZTDNR up spin in the present of barrier inside the device

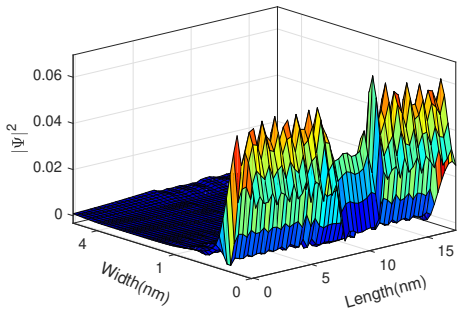

Figure 10: Electron density profile for ZTDNR down spin in the present of barrier inside the device

width of the barrier. But transmittance of the electrons is always 2 and does not depend on the height and width of the barrier. Therefore this phenomenon is Klein tunneling and this is coming from linear dispersion relationship of topological states.

4.4. Transport in the presence of constriction inside the device

We have introduced constriction in the device by removing a chunk of atoms from the channel. This is done to observe how the electron wave nature behaves in the presence of an extreme disturbance. We have shown an electron density profile in fig.11 with the presence of constriction.

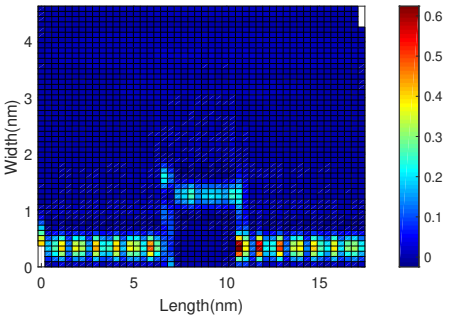

Figure 11: Electron density profile for ZTDNR with constriction

In fig.11, We observe that transportation is not affected by the existence of constriction inside the device and the electrons can pass following the edges of constriction and conduct with full transmittance (T=2). The electrons are not back scattered. This is coming from transport of topological edge states.

4.5. Transport in the presence of edge imperfections in one edge of the device

Edge imperfections can affect the transmission of the electrons through the device. First we demonstrate a plot of transmittance vs energy without SOC in fig.12.

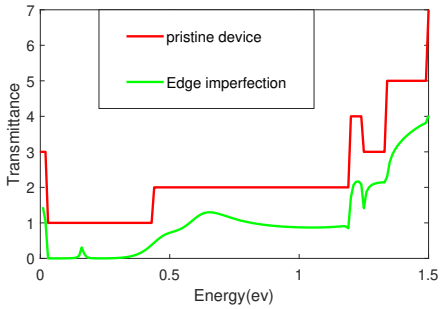

Figure 12: Transmittance vs energy without SOC for ZTDNR

From Fig.12, We observe that transmittance of the electrons is being affected by edge imperfections. Transmittance with edge imperfections is smaller than that of

the pristine device for the whole energy range. Then in fig.13, we have presented the plot of transmittance vs energy with SOC. Here the transmittance with edge

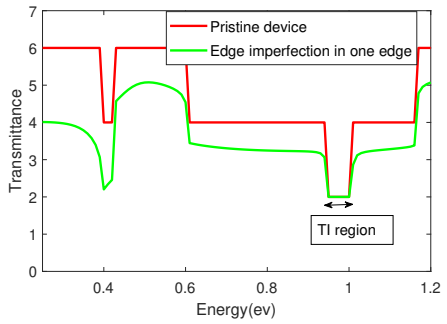

Figure 13: Transmittance vs energy with SOC for ZTDNR

imperfections in one edge is still smaller than transmittance of the pristine device for most of the energy range. In our device, electrons travel from left lead to right lead. During its travel, it faces obstacle at the presence of edge imperfections and these obstacles cause reflection of electrons. Therefore, the electrons cannot conduct with full transmittance and transmittance of the electrons decreases. We get a small energy range from 0.95ev to 1eV for which transmittance remain same as pristine device without being affected by edge imperfections. This is the TI energy range for 16-ZTDNR.

We have also presented two electron density profiles in ZTDNR for up spin and down spin with edge imperfections for this energy range in fig.14 and in fig.15 respectively. The electron density profiles in fig.14 and fig.14 show us that electrons can transport along the edge avoiding the imperfections with full transmittance (T=1) at the edge of the NR. The total transmittance of both spin electrons is 2.

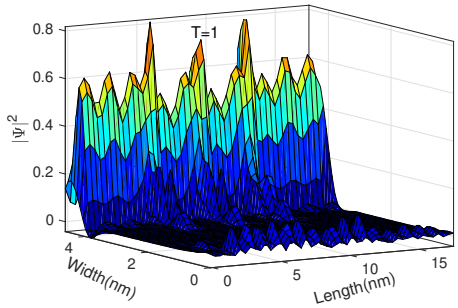

Figure 14: Electron density profile for ZTDNR up spin with edge imperfections in one edge (T=1)

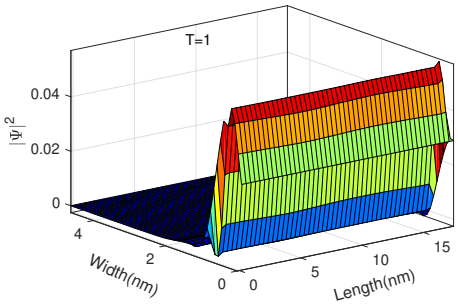

Figure 15: Electron density profile for ZTDNR down spin with edge imperfections in one edge (T=1)

4.6. Transport in the presence of edge imperfections in both edges of the device

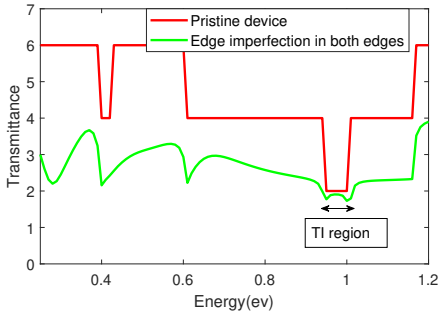

Figure 16: Transmittance vs energy with SOC for ZTDNR with imperfections in both edges

In this section, we have investigated the transport property of ZTDNR with edge imperfections in both edges of the device. We have demonstrated a plot of transmittance vs energy with SOC in fig.16.

In fig.16, we have observed that transmittance for TI energy region is being affected and is getting decreased by edge imperfections. But in fig.13, we observe that transmittance of TI energy region is not affected by edge imperfections in one edge of the device. We have also demonstrated the electron density profile of ZTDNR for up spin and down spin with edge imperfections in both edges of the device for TI energy region in fig.17 and in fig.18 respectively.

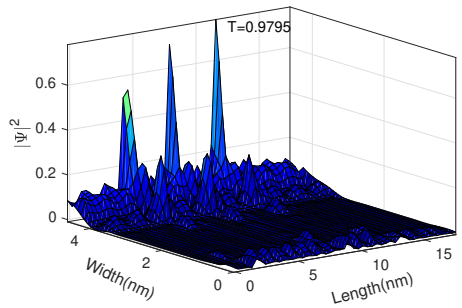

Figure 17: Electron density profile for ZTDNR up spin with edge imperfections in both edges (T=1.959)

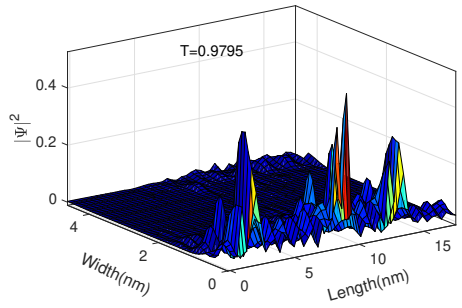

Figure 18: Electron density profile for ZTDNR down spin with edge imperfections in both edges (T=1.959)

In the above figures, we have observed the localized anderson states ([37]) around imperfections. Then we observe that electrons can transport along the edge avoiding the imperfections and the total transmittance of both spin electrons is 1.959.

5. Conclusion

We have found that zigzag edge nanoribbon of Tungsten Ditelluride with intrinsic SOC assumes topological insulator properties. The topological insulator states are quantum spin hall states. They show the characteristic edge states. It is interesting that the zigzag edge nanoribbon of Tungsten ditelluride shows edge states and klein tunneling even without intrinsic SOC, though these edge states do not show topological properties. We have shown computational results for transport in ZTDNR in the presence of constriction, potential barrier and edge imperfections. These results confirm the TI properties of ZTDNR. Interestingly when we put imperfections in one edge only, the NR shows perfect transmittance but when we put imperfections in both edges, the transmittance decreases. At present, we do not have any explanation for this behavior. But we think there is more intricacies involved in the transport of electrons in ZTDNR that need to be investigated.

References

[1] Geim, A., Grigorieva, I.: Van der Waals heterostructures. Nature 499, 419–425 (2013). https://doi.org/10.1038/nature12385

[2] Wang, Q. H., Kalantar-Zadeh, K., Kis, A., Coleman, J. N., Strano, M. S.: Electronics and optoelectronics of two-dimensional transition metal dichalcogenides. Nature nanotechnology, 7(11), 699-712(2012). https://doi.org/10.1038/nnano.2012.193

[3] Butler, Sheneve Z., Hollen, Shawna M., Cao, Linyou, Cui, Yi, Gupta, Jay A., Gutiérrez, Humberto R., Heinz, Tony F., Hong, Seung Sae, Huang, Jiaxing, Ismach, Ariel F., Johnston-Halperin, Ezekiel, Kuno, Masaru, Plashnitsa, Vladimir V., Robin-

son, Richard D., Ruoff, Rodney S., Salahuddin, Sayeef, Shan, Jie, Shi, Li, Spencer, Michael G., Terrones, Mauricio, Windl, Wolfgang, Goldberger, Joshua E.: Progress, Challenges, and Opportunities in Two-Dimensional Materials Beyond Graphene. ACS Nano, 7(4), 2898–2926(2013).
https://doi:10.1021/nn400280c

[4] Radisavljevic, B., Radenovic, A., Brivio, J., Giacometti, V., Kis, A.: Single-layer MoS2 transistors. Nature Nanotechnology, 6(3), 147–150(2011).
https://doi.org/10.1038/nnano.2010.279

[5] Xiao, Di; Liu, Gui-Bin; Feng, Wanxiang; Xu, Xiaodong; Yao, Wang: Coupled Spin and Valley Physics in Monolayers of MoS2 and Other Group-VI Dichalcogenides. , 108(19), 1968020(2012).
https://doi:10.1103/physrevlett.108.196802

[6] Sie, Edbert J., James W. McIver, Yi-Hsien Lee, Liang Fu, Jing Kong, and Nuh Gedik.: Valley-Selective Optical Stark Effect in Monolayer WS_2. Nat Mater 14, no. 3 (December 15, 2014): 290–294.
https://doi.org/10.1007/978-3-319-69554-9$_4$

[7] Li, Guohong; Luican, A.; Lopes dos Santos, J. M. B.; Castro Neto, A. H.; Reina, A.; Kong, J.; Andrei, E. Y.:Observation of Van Hove singularities in twisted graphene layers. , 6(2), 109–113.
https://doi:10.1038/nphys1463

[8] Ahmed, S., Yi, J. : Two-Dimensional Transition Metal Dichalcogenides and Their Charge Carrier Mobilities in Field-Effect Transistors. Nano-Micro Letters, 9(4), 2017.
http// doi:10.1007/s40820-017-0152-6

[9] Kumar, Rahul and Goel, Neeraj and Hojamberdiev, Mirabbos and Kumar, Mahesh:Transition metal dichalcogenides-based flexible gas sensors.Sensors and Actuators A: Physical,303,111875(2020)
https://doi.org/10.1016/j.sna.2020.111875

[10] Kim, Youngjun and Lee, Sangyoon and Song, Jeong-Gyu and Ko, Kyung Yong and Woo, Whang Je and Lee, Suk Woo and Park, Minwoo and Lee, Hoonkyung and Lee, Zonghoon and Choi, Hyunyong and others:2D Transition Metal Dichalcogenide Heterostructures for p-and n-Type Photovoltaic Self-Powered Gas Sensor.Advanced Functional Materials,30(43),2003360,(2020)
https://doi.org/10.1002/adfm.202003360

[11] Chen, Xiaoyan and Liu, Chengbin and Mao, Shun:Environmental Analysis with 2D Transition-Metal Dichalcogenide-Based Field-Effect Transistors,Nano-Micro Letters,12(1–12),(2020)
https://doi.org/10.1007/s40820-020-00438-w

[12] Iqbal, MW and Elahi, E and Amin, Aliya and Hussain, G and Aftab, Sikandar:Chemical doping of transition metal dichalcogenides (TMDCs) based field effect transistors: A review,Superlattices and Microstructures,137(106350),(2020)
https://doi.org/10.1016/j.spmi.2019.106350

[13] Hus, Saban M and Ge, Ruijing and Chen, Po-An and Liang, Liangbo and Donnelly, Gavin E and Ko, Wonhee and Huang, Fumin and Chiang, Meng-Hsueh and Li, An-Ping and Akinwande, Deji:Observation of single-defect memristor in an MoS 2 atomic sheet,Nature Nanotechnology,(1–5),(2020)
https://doi.org/10.1038/s41565-020-00789-w

[14] Shi, Y., Kahn, J., Niu, B., Fei, Z., Sun, B., Cai, X., Francisco, B. A., Wu, D., Shen, Z., Xu, X., Cobden, D. H., Cui, Y.: Imaging quantum spin Hall edges in monolayer WTe_2. Science Advances, 5(2), eaat8799(2019).
https ://doi:10.1126/sciadv.aat8799

[15] Avron, J.E., Osadchy, D., Seiler, R.: A Topological look at the Quantum Hall Efect. Phys. Today 56(8), 38–42 (2003).
https ://doi.org/10.1063/1.16113 51

[16] He, M., Sun, H., He, Q.L.: Topological insulator : spintronics and quantum computation. Front. Phys. (2019).
https://doi.org/10.1007/s11467-019-0893-4

[17] Wang, K.L., Lang, M., Kou, X.: Spintronics of Topological Insulator. Hand book of spintronics, vol. 431. (2016).
https://doi.org/10.1007/978-94-007-7604-3-6-

[18] Magarill, L.I., Entina, M.V.: Backscattering in a 2DTopological Insulator and the Conductivity of a 2D Strip. Pleiades Publishing, Inc. Letters. 100(9), 561–565 (2014).
https://doi.org/10.1134/S0021364014210097

[19] Moore, J.E.: The birth of topological insulator. Nature 464, 194–198 (2010).
https://doi.org/10.1038/nature08916

[20] Marcin Kurpas, M., Faria Jr. P. E., Gmitra , M., Fabian, J. : Spin-orbit coupling in elemental two-dimensional materials. Physical Review B 100, 125422, 2019.

https://doi.org/10.1103/PhysRevB.100.125422

[21] Braz, J.E.H., Vieira de Castro, E.F., Peres, N.M.R. :Electronic Properties of Single-layered Transition Metal Dichalcogenides . Department of Physics, Instituto Superior T ecnico, Universidade de Lisboa, Av. Rovisco Pais, 1049-001 Lisboa, Portugal (2015).

[22] Liu, P., Williams, J.R., Chan, J.J.: Topological nanomaterials.Nat. Rev. Mater. 4, 479–496 (2019).
https://doi.org/10.1038/s41578-019-0113-4

[23] Kin, M., Changgu, L., James, H., Jie,S., Tony, H.: Atomically Thin MoS_2: A New Direct-Gap Semiconductor. , 105(13), 1368050(2010).
https://doi.org/10.1103/PhysRevLett.105.136805

[24] Xu, Su-Yang and Ma, Qiong and Shen, Huitao and Fatemi, Valla and Wu, Sanfeng and Chang, Tay-Rong and Chang, Guoqing and Valdivia, Andrés M Mier and Chan, Ching-Kit and Gibson, Quinn D and others:Electrically switchable Berry curvature dipole in the monolayer topological insulator WTe 2,Nature Physics volume 14, pages 900-906(2018)
https://doi.org/10.1038/s41567-018-0189-6

[25] Shi, Yanmeng and Kahn, Joshua and Niu, Ben and Fei, Zaiyao and Sun, Bosong and Cai, Xinghan and Francisco, Brian A and Wu, Di and Shen, Zhi-Xun and Xu, Xiaodong and others:Imaging quantum spin Hall edges in monolayer WTe2, Science Advances 5, eaat8799 (2019)
DOI: 10.1126/sciadv.aat8799

[26] Alam, M., Voss, P.L.: Graphene quantum interference photodetector. Beilstein J. Nanotechnol. 6, 726–735 (2015).
https://doi.org/10.3762/bjnano.6.74

[27] Vogl, P., Kubis, T.: The non-equilibrium Green's function method: an introduction. J. Comput. Electron. 9, 237–242 (2010).
https://doi.org/10.1007/s10825-010-0313-z

[28] Wang, Q. H., Kalantar-Zadeh, K., Kis, A., N. Coleman, J., S. Strano., M. : Electronics and optoelectronics of two-dimensional transition metal dichalcogenides. Nat Nano, 7(11):699–712, 11, 2012.

[29] Datta, S.: Quantum Transport: Atom to Transistor, 1st ed. Cambridge University Press, UK(2005).

[30] Datta, S.: Electronic Transport in Mesoscopic Systems, 5th ed. Cambridge University Press, UK(2003).

[31] Datta, S.:Lessons from Nanoelectronics- A New Perspective on Transport. World Scientific.USA(2012).

[32] Datta, S.: Superlattices Microstruct. 28, 253-278(2000).
https://doi:10.1006/spmi.2000.0920

[33] Liu, G., Shan, W., Yao, Y., Yao, W.,Di, X.: Three-band tight-binding model for monolayers of group-VIB transition metal dichalcogenides. Physical Review B, 88(8), 085433 (2013).
https://doi.org/10.1103/PhysRevB.88.085433

[34] Alam, M.: Nanoscale optical devices based on phase coherent electron transport. PhD Thesis. School of Electrical and Computer Engineering Georgia Institute of Technology. Georgia (2016).

[35] Yu, J., Zhong, J., Kuang, X. et al. Dynamic Control of High-Range Photoresponsivity in a Graphene Nanoribbon Photodetector. Nanoscale Res Lett 15, 124 (2020).
https://doi.org/10.1186/s11671-020-03352-7

[36] Jeon, K.-R., Jeon, J.-C., Zhou, X., Migliorini, A., Yoon, J., Parkin, S. S. P.: Giant Transition-State Quasiparticle Spin-Hall Effect in an Exchange-Spin-Split Superconductor Detected by Nonlocal Magnon Spin Transport. ACS Nano, 22, 85-107(2020).
https://doi:10.1021/acsnano.0c07187

[37] Park, Jungmin and Oh, Inseon and Jin, Mi-Jin and Jo, Junhyeon and Choe, Daeseong and Yun, Hyung Duk and Lee, Suk Woo and Lee, Zonghoon and Kwon, Soon-Yong and Jin, Hosub and others:Observation of spin-polarized Anderson state around charge neutral point in graphene with Fe-clusters,Scientific reports,10(1),(1–8),(2020).
https://doi.org/10.1038/s41598-020-61481-6